

Tunable quantum gate between a superconducting atom and a propagating microwave photon

K. Koshino,¹ K. Inomata,² Z. R. Lin,² Y. Tokunaga,³ T. Yamamoto,⁴ and Y. Nakamura^{2,5}

¹College of Liberal Arts and Sciences, Tokyo Medical and Dental University, Ichikawa, Chiba 272-0827, Japan

²RIKEN Center for Emergent Matter Science (CEMS), 2-1 Hirosawa, Wako, Saitama 351-0198, Japan

³NTT Secure Platform Laboratories, NTT Corporation, Musashino 180-8585, Japan

⁴IoT Device Research Laboratories, NEC Corporation, Tsukuba, Ibaraki 305-8501, Japan

⁵Research Center for Advanced Science and Technology (RCAST),

The University of Tokyo, Meguro-ku, Tokyo 153-8904, Japan

(Dated: January 11, 2022)

We propose a two-qubit quantum logic gate between a superconducting atom and a propagating microwave photon. The atomic qubit is encoded on its lowest two levels and the photonic qubit is encoded on its carrier frequencies. The gate operation completes deterministically upon reflection of a photon, and various two-qubit gates (SWAP, $\sqrt{\text{SWAP}}$, and Identity) are realized through *in situ* control of the drive field. The proposed gate is applicable to construction of a network of superconducting atoms, which enables gate operations between non-neighboring atoms.

Physical implementation of a scalable quantum system that enables quantum computation is one of the main objectives in modern quantum technology. There are two approaches for achieving this goal. In the first approach, we construct a quantum circuit which is composed of qubits of the same kind: the one-qubit gates are realized by local operations on a single qubit, and the two-qubit gates are realized by mutual interaction between a pair of qubits. For example, high-fidelity gate operations reaching the fault tolerance threshold for surface code error correction [1] have been achieved in an array of superconducting qubits [2]. Recently, a scalable Shor's algorithm [3] has been demonstrated using a trapped ion quantum computer [4].

In the second approach, which is known as the distributed or modular architecture, we use a hybrid quantum network composed of flying and stationary qubits [5–10]. Flying qubits, which are typically implemented by photons, transfer quantum information among the stationary nodes. The stationary qubits, which are implemented by real or artificial atoms, are used to register and process quantum information. Construction of such hybrid quantum networks has been developed actively in cavity quantum electrodynamics (QED) using real atoms and optical photons. For example, a deterministic quantum gate between a propagating photon and an atom has been demonstrated, which has been further extended to a photon-photon gate [11–13]. The observation of single-photon Raman interaction [14, 15] would be a crucial step towards achieving the swap-based photon-photon gates [16]. Similarly, in the microwave quantum-optics setups based on circuit QED [17, 18], we can connect superconducting atoms by microwave photons propagating in waveguides. Recently, entanglement generation between two remote superconducting atoms has been achieved by interfering the two microwave photons emitted by the atoms [19].

In this study, we propose a new scheme for implementing deterministic two-qubit gates between a superconducting atom and a propagating microwave photon. In the proposed device, a driven superconducting atom is coupled to a waveguide photon via a resonator (Fig. 1). The atomic qubit is encoded on its two lowest levels ($|g\rangle$ and $|e\rangle$), and the photon qubit is encoded on its carrier frequencies [20]. The gate operation completes deterministically upon reflection of a photon. A remarkable feature of the proposed gate is its tunability: through *in situ* control of the drive field to the atom, we can continuously change the gate type, including SWAP, $\sqrt{\text{SWAP}}$, and Identity gates which are of practical importance. Furthermore, by cascading the proposed devices, we can execute an entangling gate between two remote superconducting atoms. This implies the realization of a universal gate set, since one-qubit gate operations are easy in superconducting atoms.

The schematic of the considered device is shown in Fig. 1. A superconducting artificial atom, which can be regarded as a two-level system, is dispersively coupled to a resonator. The resonator and the atom are respectively coupled to waveguides 1 and 2. Through waveguide 1, we input a microwave-photon qubit, whose quantum information is encoded on its carrier frequencies. Through waveguide 2, we apply a drive field to the atom in order to engineer the dressed states of the atom-resonator system [21]. Assuming a static drive field of amplitude Ω_d and frequency ω_d , the Hamiltonian of the atom-resonator system is given, in the rotating frame, by

$$\mathcal{H}_{ar} = \omega_r a^\dagger a \sigma \sigma^\dagger + [(\omega_a - \omega_d) + (\omega_r - 2\chi)a^\dagger a] \sigma^\dagger \sigma + \Omega_d (\sigma^\dagger + \sigma), \quad (1)$$

where σ (a) is the annihilation operator for the atom (resonator), ω_a (ω_r) is the resonance frequency of the atom (resonator), and χ is the dispersive shift. For concreteness, we assume the following parameter values: $\omega_a/2\pi = 5$ GHz, $\omega_r/2\pi = 10$ GHz, and $\chi/2\pi = 75$ MHz.

Throughout this study, we use the lowest four levels of the atom-resonator system, $|g, 0\rangle$, $|e, 0\rangle$, $|g, 1\rangle$, and $|e, 1\rangle$. These *bare* states are the eigenstates of \mathcal{H}_{ar} when the drive field is off ($\Omega_d = 0$). We set the drive frequency ω_d

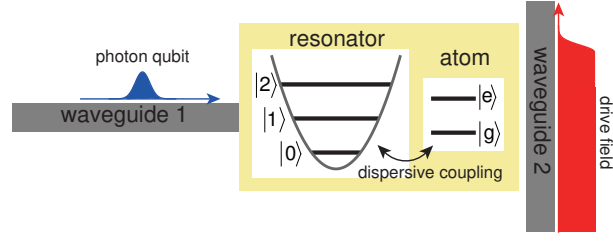


FIG. 1: Schematic of the tunable atom-photon quantum gate. We input a photon qubit through waveguide 1 and drive the superconducting atom through waveguide 2. The quantum-gate operation completes upon reflection of the photon. We can realize various types of quantum gate by changing the drive condition.

within the range of $\omega_a - 2\chi < \omega_d < \omega_a$. Then, in the frame rotating at ω_d , we obtain a nested energy diagram of the bare states, where $\omega_{|g,0\rangle} < \omega_{|e,0\rangle} < \omega_{|e,1\rangle} < \omega_{|g,1\rangle}$. When the drive field is on, the bare states are hybridized to form the dressed states. We label them from the lowest in energy and denote them by $|\tilde{1}\rangle$, $|\tilde{2}\rangle$, $|\tilde{3}\rangle$, and $|\tilde{4}\rangle$ [Fig. 2(a)]. Diagonalizing \mathcal{H}_{ar} , they are given by

$$|\tilde{1}\rangle = \cos\theta_l|g, 0\rangle - \sin\theta_l|e, 0\rangle, \quad (2)$$

$$|\tilde{2}\rangle = \sin\theta_l|g, 0\rangle + \cos\theta_l|e, 0\rangle, \quad (3)$$

$$|\tilde{3}\rangle = \cos\theta_h|e, 1\rangle - \sin\theta_h|g, 1\rangle, \quad (4)$$

$$|\tilde{4}\rangle = \sin\theta_h|e, 1\rangle + \cos\theta_h|g, 1\rangle, \quad (5)$$

where $\theta_l = \frac{1}{2}\arg(\frac{\omega_a - \omega_d}{2} + i\Omega_d)$ and $\theta_h = \frac{1}{2}\arg(\frac{\omega_d - \omega_a + 2\chi}{2} + i\Omega_d)$. Their eigenenergies are given by

$$\tilde{\omega}_{1,2} = \frac{\omega_a - \omega_d}{2} \pm \sqrt{\left(\frac{\omega_a - \omega_d}{2}\right)^2 + \Omega_d^2}, \quad (6)$$

$$\tilde{\omega}_{3,4} = \omega_r - \frac{\omega_d - \omega_a + 2\chi}{2} \pm \sqrt{\left(\frac{\omega_d - \omega_a + 2\chi}{2}\right)^2 + \Omega_d^2}, \quad (7)$$

where the plus (minus) sign is taken for $\tilde{\omega}_2$ and $\tilde{\omega}_4$ ($\tilde{\omega}_1$ and $\tilde{\omega}_3$). In this four level system, $|\tilde{3}\rangle$ and $|\tilde{4}\rangle$ decay to $|\tilde{1}\rangle$ and $|\tilde{2}\rangle$ emitting a photon into waveguide 1. Denoting the radiative decay rate of resonator by κ , the decay rates between the dressed states are given by

$$\tilde{\kappa}_{32} = \tilde{\kappa}_{41} = \kappa \cos^2\theta_t, \quad (8)$$

$$\tilde{\kappa}_{31} = \tilde{\kappa}_{42} = \kappa \sin^2\theta_t, \quad (9)$$

where $\theta_t = \theta_l + \theta_h$.

We discuss the response of this four-level system to a single microwave photon input through waveguide 1. For simplicity, we assume that the input photon is monochromatic with frequency ω . Furthermore, we assume that both $|\tilde{1}\rangle$ and $|\tilde{2}\rangle$ are stable and the four-level system is in their superposition initially. Due to the oblique decay paths ($\tilde{\kappa}_{31}$ and $\tilde{\kappa}_{42}$), the input photon may induce the Raman transition upon reflection. The state vector of the overall system, consisting of a propagating photon and the dressed states, evolves as

$$|\tilde{1}, \omega\rangle \rightarrow \xi_{11}(\omega)|\tilde{1}, \omega\rangle + \xi_{12}(\omega)|\tilde{2}, \omega - \Delta\omega\rangle, \quad (10)$$

$$|\tilde{2}, \omega\rangle \rightarrow \xi_{21}(\omega)|\tilde{1}, \omega + \Delta\omega\rangle + \xi_{22}(\omega)|\tilde{2}, \omega\rangle, \quad (11)$$

where $\Delta\omega = \tilde{\omega}_{21} = \tilde{\omega}_2 - \tilde{\omega}_1$. The coefficients ξ_{ij} are given by (see Appendix A)

$$\xi_{11}(\omega) = 1 - \frac{\kappa \sin^2\theta_t}{\frac{\kappa}{2} - i(\omega - \tilde{\omega}_{31})} - \frac{\kappa \cos^2\theta_t}{\frac{\kappa}{2} - i(\omega - \tilde{\omega}_{41})}, \quad (12)$$

$$\xi_{12}(\omega) = \frac{\kappa \sin\theta_t \cos\theta_t}{\frac{\kappa}{2} - i(\omega - \tilde{\omega}_{31})} - \frac{\kappa \sin\theta_t \cos\theta_t}{\frac{\kappa}{2} - i(\omega - \tilde{\omega}_{41})}, \quad (13)$$

$$\xi_{21}(\omega) = \frac{\kappa \sin\theta_t \cos\theta_t}{\frac{\kappa}{2} - i(\omega - \tilde{\omega}_{32})} - \frac{\kappa \sin\theta_t \cos\theta_t}{\frac{\kappa}{2} - i(\omega - \tilde{\omega}_{42})}, \quad (14)$$

$$\xi_{22}(\omega) = 1 - \frac{\kappa \cos^2\theta_t}{\frac{\kappa}{2} - i(\omega - \tilde{\omega}_{32})} - \frac{\kappa \sin^2\theta_t}{\frac{\kappa}{2} - i(\omega - \tilde{\omega}_{42})}. \quad (15)$$

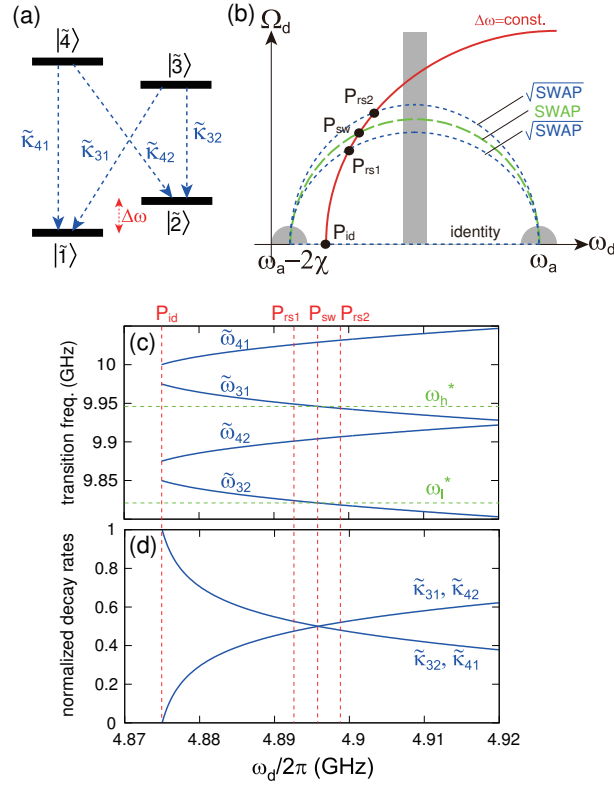


FIG. 2: Dressed-state engineering. (a) Level structure of the dressed states in the rotating frame. (b) Drive conditions to achieve various quantum gates. We change the drive condition along the red solid line, where $\Delta\omega = \tilde{\omega}_{21}$ is kept constant. SWAP gate is realized at P_{sw} , $\sqrt{\text{SWAP}}$ is realized at $P_{rs1/2}$, and Identity gate is realized at P_{id} . In the shadowed areas, the gate fidelities are degraded due to the parasitic excitations. (c) Transition frequencies $\tilde{\omega}_{ij}$ and (d) normalized decay rates $\tilde{\kappa}_{ij}/\kappa$ as functions of ω_d . Ω_d is adjusted to satisfy $\Delta\omega/2\pi = 125$ MHz.

We can confirm the probability conservation, $|\xi_{11}|^2 + |\xi_{12}|^2 = |\xi_{21}|^2 + |\xi_{22}|^2 = 1$.

In the proposed atom-photon gate, we use $|\tilde{1}\rangle$ and $|\tilde{2}\rangle$ as the logical basis for the material node. Note that these states are roughly the atomic ground and excited states ($|\tilde{1}\rangle \approx |g, 0\rangle$ and $|\tilde{2}\rangle \approx |e, 0\rangle$) under our choice of the drive condition. For the photonic qubit, we encode quantum information on its carrier frequency: the basis states are $|\omega_l\rangle$ and $|\omega_h\rangle$, where $(\omega_l, \omega_h) = (\tilde{\omega}_{32}, \tilde{\omega}_{31})$ or $(\tilde{\omega}_{42}, \tilde{\omega}_{41})$. For concreteness, we focus on the former case and use $|\tilde{1}\rangle$, $|\tilde{2}\rangle$ and $|\tilde{3}\rangle$ as a Λ system hereafter. The case of an ‘‘impedance-matched’’ Λ system, where $\theta_t = \pi/4$ and therefore $\tilde{\kappa}_{31} = \tilde{\kappa}_{32}$, is of particular importance. If $\omega_l (= \tilde{\omega}_{32})$ is detuned sufficiently from the non-target transitions ($\tilde{\omega}_{31}$, $\tilde{\omega}_{41}$, and $\tilde{\omega}_{42}$), we immediately observe in Eqs. (12)–(15) that $\xi_{11}(\omega_l) = \xi_{21}(\omega_l) = 1$ and $\xi_{12}(\omega_l) = \xi_{22}(\omega_l) = 0$, which implies that $|\tilde{1}, \omega_l\rangle \rightarrow |\tilde{1}, \omega_l\rangle$ and $|\tilde{2}, \omega_l\rangle \rightarrow |\tilde{1}, \omega_h\rangle$. Similarly, $|\tilde{1}, \omega_h\rangle \rightarrow |\tilde{2}, \omega_l\rangle$ and $|\tilde{2}, \omega_h\rangle \rightarrow |\tilde{2}, \omega_h\rangle$. These four time evolutions are summarized as

$$(\alpha_1|\tilde{1}\rangle + \alpha_2|\tilde{2}\rangle) \otimes (\beta_1|\omega_l\rangle + \beta_2|\omega_h\rangle) \rightarrow (\beta_1|\tilde{1}\rangle + \beta_2|\tilde{2}\rangle) \otimes (\alpha_1|\omega_l\rangle + \alpha_2|\omega_h\rangle). \quad (16)$$

where α_1 , α_2 , β_1 and β_2 are arbitrary coefficients. Namely, SWAP gate is achieved between the photon and atom qubits. Note that the deterministic Raman transition, $|\tilde{1}, \omega_h\rangle \rightarrow |\tilde{2}, \omega_l\rangle$, has been demonstrated recently as the deterministic down-conversion and is applied for detection of single microwave photons [22, 23].

The frequency ω_d and the amplitude Ω_d of the qubit drive are chosen as follows: (i) In order to constitute an impedance-matched Λ system ($\theta_t = \pi/4$), ω_d and Ω_d should satisfy

$$4\Omega_d^2 = (\omega_a - \omega_d)(\omega_d - \omega_a + 2\chi). \quad (17)$$

This is represented as an ellipse on the (ω_d, Ω_d) plane [green dashed line in Fig. 2(b)]. (ii) $\omega_l (= \tilde{\omega}_{32})$ and $\omega_h (= \tilde{\omega}_{31})$ should be detuned sufficiently from the non-target transitions. This requires that $(\omega_d, \Omega_d) \neq (\omega_a - 2\chi, 0)$, $(\omega_d, \Omega_d) \neq (\omega_a, 0)$, and $\omega_d \neq \omega_a - \chi$ [shadowed areas in Fig. 2(b)]. (iii) The frequency difference between the two basis states,

$\Delta\omega = \omega_h - \omega_l$ is given, from Eq. (6), by

$$\Delta\omega = \sqrt{(\omega_a - \omega_d)^2 + 4\Omega_d^2}. \quad (18)$$

The condition that $\Delta\omega = \text{constant}$ is also represented as an ellipse on the (ω_d, Ω_d) plane [red solid line in Fig. 2(b)]. Practically, a large $\Delta\omega$ is advantageous, since we can suppress the effects of finite qubit lifetime by using a short photon pulse. Hereafter we set $\Delta\omega/2\pi = 125$ MHz. From Eqs. (17) and (18), the drive condition to achieve a SWAP gate is determined as

$$\omega_d^{\text{sw}} = \omega_a - \frac{(\Delta\omega)^2}{2\chi}, \quad (19)$$

$$\Omega_d^{\text{sw}} = \frac{\Delta\omega}{4\chi} \sqrt{4\chi^2 - (\Delta\omega)^2}, \quad (20)$$

which amount to $\omega_d^{\text{sw}}/2\pi = 4.896$ GHz and $\Omega_d^{\text{sw}}/2\pi = 34.55$ MHz, respectively [P_{sw} in Fig. 2(b)]. With this qubit drive, the carrier frequencies of the photon qubit are determined as

$$\omega_l^* = \omega_r - \chi - \sqrt{\chi^2 - \left(\frac{\Delta\omega}{2}\right)^2} - \frac{\Delta\omega}{2}, \quad (21)$$

$$\omega_h^* = \omega_r - \chi - \sqrt{\chi^2 - \left(\frac{\Delta\omega}{2}\right)^2} + \frac{\Delta\omega}{2}, \quad (22)$$

which amounts to $\omega_l^*/2\pi = 9.821$ GHz and $\omega_h^*/2\pi = 9.946$ GHz, respectively [Fig. 2(c)].

A merit of the present scheme is that the transition frequencies and the decay rates between the dressed states are controllable through the drive field. In particular, we can vary the drive condition conserving the frequency difference $\Delta\omega$ between $|\tilde{1}\rangle$ and $|\tilde{2}\rangle$ [solid line in Fig. 2(b)]. By changing the drive condition smoothly with a transit time of the order of 10 ns, we can suppress the non-adiabatic transition between $|\tilde{1}\rangle$ and $|\tilde{2}\rangle$. This implies that various atom-photon gates can be realized without changing the logical basis. For example, when the qubit drive is off [P_{id} of Fig. 2(b)], $\Omega_d = 0$ and therefore $\theta_t = 0$. Then we realize an Identity gate, where the atom and photon qubits remain unchanged upon reflection. Furthermore, under different drive conditions [P_{rs1} and P_{rs2} of Fig. 2(b)], we realize a $\sqrt{\text{SWAP}}$ gate, which generates maximal entanglement between the atom and photon qubits [24]. The basis states evolve as $|\tilde{1}, \omega_l^*\rangle \rightarrow |\tilde{1}, \omega_l^*\rangle$, $|\tilde{1}, \omega_h^*\rangle \rightarrow \frac{1+i}{2}|\tilde{1}, \omega_h^*\rangle + \frac{1-i}{2}|\tilde{2}, \omega_l^*\rangle$, $|\tilde{2}, \omega_l^*\rangle \rightarrow \frac{1-i}{2}|\tilde{1}, \omega_h^*\rangle + \frac{1+i}{2}|\tilde{2}, \omega_l^*\rangle$, and $|\tilde{2}, \omega_h^*\rangle \rightarrow |\tilde{2}, \omega_h^*\rangle$, where the upper (lower) signs should be taken at P_{rs1} (P_{rs2}).

In the above discussions, the lifetime T_1 of the superconducting atom and the length l of the photon pulse are assumed to be infinite. Here, taking account of their finiteness, we evaluate the gate fidelity quantitatively. We assume a long-lived superconducting atom with $T_1 = 80$ μs and with negligible pure dephasing, and employ a trigonometric pulse profile for the photon qubit, as given by

$$f_{\omega,l}(t) = \begin{cases} \sqrt{2/l} \cos(\pi t/l) \exp(-i\omega t) & (|t| < l/2) \\ 0 & (\text{otherwise}), \end{cases} \quad (23)$$

where $\omega = \omega_l^*$ or ω_h^* . Note that a pulse-shaped single photon is available in the microwave domain [25]. For $\Delta\omega/2\pi = 125$ MHz, by choosing the pulse length $l \gtrsim 50$ ns, the overlap between $|\omega_h\rangle$ and $|\omega_l\rangle$ in the frequency space becomes negligible ($|\langle\omega_l^*|\omega_h^*\rangle| \lesssim 10^{-3}$). Setting the initial moment at $t = -l/2$, we evaluate an averaged gate fidelity after photon reflection at $t = l/2$. In Fig. 3, the average gate fidelities of SWAP and Identity gates are plotted as functions of κ and l (see Appendix B). The conditions for high-fidelity SWAP gate are (i) the gate time l is much shorter than the lifetime T_1 of the atom, (ii) the delay of the photon pulse due to absorption and reemission ($\sim \kappa^{-1}$) is much smaller than the pulse length l , and (iii) levels $|\tilde{3}\rangle$ and $|\tilde{4}\rangle$ are well resolved in frequency, which requires $\kappa \ll \tilde{\omega}_{43} \simeq 2\pi \times 70$ MHz [see Fig. 2(c)]. On the other hand, the conditions for high-fidelity Identity gate are (i) and (iv) the carrier frequencies ω_l^* and ω_h^* are detuned sufficiently from $\tilde{\omega}_{32}$ and $\tilde{\omega}_{41}$, which requires $\kappa \ll |\tilde{\omega}_{32} - \omega_l^*| \simeq 2\pi \times 30$ MHz [see Fig. 2(c)]. By setting $\kappa/2\pi = 5.236$ MHz and $l = 1.738$ μs , the gate fidelities reach $\mathcal{F}_{\text{id}} = 0.986$, $\mathcal{F}_{\text{sw}} = 0.980$, $\mathcal{F}_{\text{rs1}} = 0.986$, and $\mathcal{F}_{\text{rs2}} = 0.986$. These fidelities are sufficient for the communication channel in the distributed architecture [8]. We can further improve the gate fidelities by enhancing the lifetime T_1 of the atom and the dispersive shift χ .

By cascading such atom-resonator systems using circulators [Fig. 4(a)], we build up a one-dimensional network of atomic qubits which are connected quantum-mechanically by propagating photons. For example, we present the circuit diagram of a ‘‘quantum domino’’ in Fig. 4(b). We set the drive conditions of all atoms at P_{sw} of Fig. 2(b). All atomic qubits are in arbitrary states initially, and an arbitrary photon qubit is input into this circuit. Then, the input photon qubit is swapped with the atomic ones successively. As a result, all atomic qubits are transferred to the succeeding ones after passage of the photon. If desired, we can skip specific atoms in this domino by switching off

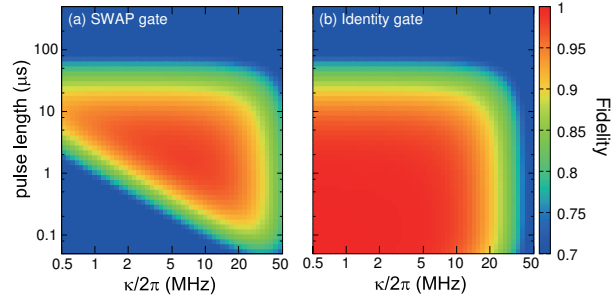


FIG. 3: Average gate fidelities for (a) SWAP and (b) Identity gates as functions of the linewidth κ of the resonator and the pulse length l .

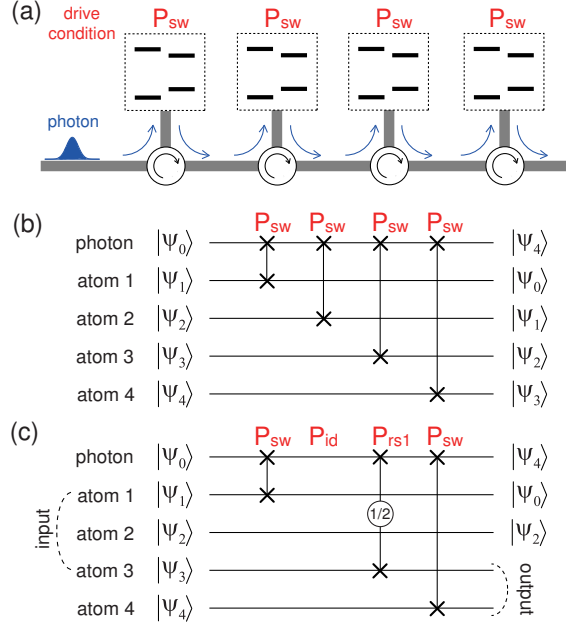


FIG. 4: One-dimensional quantum circuit. (a) Schematic of the circuit. Superconducting atoms are cascaded by circulators. The drive conditions of the atoms are individually controllable. (b) Circuit diagram of the quantum domino. (c) Circuit diagram of the atom-atom $\sqrt{\text{SWAP}}$ gate. The input qubits are atoms 1 and 3, and the output qubits are atoms 3 and 4.

their drive fields [P_{id} of Fig. 2(b)]. As another example, we present the circuit diagram of atom-atom $\sqrt{\text{SWAP}}$ gate in Fig. 4(c). We set the drive conditions of atoms 1 to 4 at P_{sw} , P_{id} , $P_{\text{rs}1/2}$, and P_{sw} , respectively. All atomic qubits are in arbitrary states initially, and an arbitrary photon qubit is input into this circuit. Then, the input photon qubit is swapped with atom 1, skips atom 2, becomes entangled with atom 3, and is swapped again with atom 4. This results in the atom-atom $\sqrt{\text{SWAP}}$ gate, where the input (output) qubits are atoms 1 and 3 (3 and 4): $|\tilde{1}, \tilde{1}\rangle_{13} \rightarrow |\tilde{1}, \tilde{1}\rangle_{34}$, $|\tilde{1}, \tilde{2}\rangle_{13} \rightarrow \frac{1 \mp i}{2} |\tilde{1}, \tilde{2}\rangle_{34} + \frac{1 \pm i}{2} |\tilde{2}, \tilde{1}\rangle_{34}$, $|\tilde{2}, \tilde{1}\rangle_{13} \rightarrow \frac{1 \pm i}{2} |\tilde{1}, \tilde{2}\rangle_{34} + \frac{1 \mp i}{2} |\tilde{2}, \tilde{1}\rangle_{34}$, and $|\tilde{2}, \tilde{2}\rangle_{13} \rightarrow |\tilde{2}, \tilde{2}\rangle_{34}$. The initial qubits of photon and atom 4 are transferred to atom 1 and photon, respectively, and atom 2 remains unchanged.

The proposed quantum network has the following distinct advantages. (i) The gate type can be controlled *in situ* through the atomic drive, without changing the circuit configuration nor the carrier frequencies ω_l^* and ω_h^* of the photonic qubits. (ii) As a source of input photons, a monochromatic single-photon generator at ω_l^* or ω_h^* is sufficient, since this photon can be reset to a desired state by swapping with atom 1. (iii) One can skip arbitrary atoms in the circuit by switching off their drive fields [for example, atom 2 in Fig. 4(c)]. This implies the possibility of two-qubit gates between non-neighboring qubits, which would substantially simplify the gate-based quantum computation. (iv) One-qubit gate operations to individual atoms are readily performable through the drive fields. Therefore, combined with the $\sqrt{\text{SWAP}}$ gate, the universal gate set is completed in the atomic network. We can perform universal quantum computation by inputting microwave photons successively and varying the drive conditions.

In summary, we theoretically proposed a two-qubit gate between a superconducting atom and a propagating microwave photon. The gate operation completes deterministically upon reflection of the photon, and various two-qubit gates (including SWAP, $\sqrt{\text{SWAP}}$, and Identity) are realizable through *in situ* control of the drive field. We can construct a quantum network of superconducting atoms aided by microwave photons, in which two-qubit gates are performable between non-neighboring atoms. This would widen the potential of superconducting quantum computing.

This work was partly supported by JSPS KAKENHI (Grants No. 16K05497, No. 26220601, and No. 15K17731).

Appendix A: Derivation of $\xi_{ij}(\omega)$

Here, we derive the coefficients $\xi_{ij}(\omega)$ which appear in Eqs. (12)–(15). The Hamiltonian of the overall system including waveguide 1 is given by

$$\mathcal{H} = \mathcal{H}_{ar} + \mathcal{H}_{rw}, \quad (\text{A1})$$

$$\mathcal{H}_{ar} = \omega_r a^\dagger a \sigma \sigma^\dagger + [(\omega_q - \omega_d) + (\omega_r - 2\chi) a^\dagger a] \sigma^\dagger \sigma + \Omega_d (\sigma^\dagger + \sigma), \quad (\text{A2})$$

$$\mathcal{H}_{rw} = \int dk \left[k a_k^\dagger a_k + \sqrt{\kappa/2\pi} (a^\dagger a_k + a_k^\dagger a) \right], \quad (\text{A3})$$

where \mathcal{H}_{ar} describes the driven atom-resonator system [Eq. (1)], \mathcal{H}_{rw} describes the interaction between the resonator and the propagating photon in waveguide 1, and a_k is the annihilation operator of the waveguide photon with wave number k . The superconducting atom is assumed to have an infinite lifetime here. Switching to the dressed-state basis [Eqs. (2)–(5)], \mathcal{H} is rewritten as

$$\mathcal{H} = \sum_j \tilde{\omega}_j \sigma_{jj} + \int dk \left[k a_k^\dagger a_k + \sum_{i,j} (\eta_{ji} \sigma_{ji} a_k + \eta_{ji}^* a_k^\dagger \sigma_{ij}) / \sqrt{2\pi} \right], \quad (\text{A4})$$

where the indices run over $i, j = 1, \dots, 4$ and $\sigma_{ji} = |\tilde{j}\rangle\langle\tilde{i}|$. η_{ji} is given by $\eta_{32} = \eta_{41} = \sqrt{\kappa} \cos \theta_t$, $\eta_{42} = -\eta_{31} = \sqrt{\kappa} \sin \theta_t$, and $\eta_{ji} = 0$ otherwise.

We introduce the real-space representation of the field operator by $a_r = (2\pi)^{-1/2} \int dk e^{ikr} a_k$. In this representation, the $r < 0$ ($r > 0$) region corresponds to the incoming (outgoing) field. From Eq. (A4), we can rigorously derive the following input-output relation,

$$a_r(t) = a_{r-t}(0) - i\theta(r)\theta(t-r) \sum_{i,j} \eta_{ji}^* \sigma_{ij}(t-r), \quad (\text{A5})$$

where $\theta(r)$ is the Heaviside step function. We can also derive the following Heisenberg equations,

$$\frac{d}{dt} \sigma_{13} = (-i\tilde{\omega}_{31} - \kappa/2) \sigma_{13} + i[\eta_{31}(\sigma_{33} - \sigma_{11}) - \eta_{32}\sigma_{12} + \eta_{41}\sigma_{43}] a_{-t}(0), \quad (\text{A6})$$

$$\frac{d}{dt} \sigma_{14} = (-i\tilde{\omega}_{41} - \kappa/2) \sigma_{14} + i[\eta_{41}(\sigma_{44} - \sigma_{11}) - \eta_{42}\sigma_{12} + \eta_{31}\sigma_{34}] a_{-t}(0), \quad (\text{A7})$$

where $\tilde{\omega}_{ij} = \tilde{\omega}_i - \tilde{\omega}_j$.

Hereafter, we consider a case in which the atom is in the state $|\tilde{1}\rangle$ and a single photon with wavefunction $f(r)$ is input at the initial moment ($t = 0$). The initial and final state vectors are written as

$$|\phi_{in}\rangle = \int dr f(r) a_r^\dagger |\tilde{1}\rangle, \quad (\text{A8})$$

$$|\phi_{out}\rangle = e^{-i\tilde{\omega}_1 t} \int dr g_{11}(r, t) a_r^\dagger |\tilde{1}\rangle + e^{-i\tilde{\omega}_2 t} \int dr g_{12}(r, t) a_r^\dagger |\tilde{2}\rangle, \quad (\text{A9})$$

where $g_{11}(r, t)$ and $g_{12}(r, t)$ are the photon wavefunctions after reflection, and the final moment t is sufficiently large. The initial and final state vectors are connected by the unitary time evolution, $|\phi_{out}\rangle = e^{-i\mathcal{H}t} |\phi_{in}\rangle$. Note that the natural time evolution of the dressed state ($e^{-i\tilde{\omega}_j t}$) is separated. For later convenience, we introduce $s_{13}(t) = \langle \tilde{1} | \sigma_{13}(t) | \phi_{in} \rangle$ and $s_{14}(t) = \langle \tilde{1} | \sigma_{14}(t) | \phi_{in} \rangle$. Their equations of motion are given, remembering that $a_{-t}(0) | \phi_{in} \rangle = f(-t) | \tilde{1} \rangle$ and that $|\tilde{1}\rangle$ is an eigenstate of \mathcal{H} , by

$$\frac{d}{dt} s_{13} = (-i\tilde{\omega}_{31} - \kappa/2) s_{13} - i\eta_{31} f(-t), \quad (\text{A10})$$

$$\frac{d}{dt} s_{14} = (-i\tilde{\omega}_{41} - \kappa/2) s_{14} - i\eta_{41} f(-t). \quad (\text{A11})$$

If the pulse length of the input photon is much larger than κ^{-1} , we can adiabatically solve the above equations. Denoting the central frequency of the input photon by ω , the adiabatic solutions are given by

$$s_{13}(t) = \frac{-i\eta_{31}}{\kappa/2 - i(\omega - \tilde{\omega}_{31})} f(-t), \quad (\text{A12})$$

$$s_{14}(t) = \frac{-i\eta_{41}}{\kappa/2 - i(\omega - \tilde{\omega}_{41})} f(-t). \quad (\text{A13})$$

From Eq. (A9), we have $g_{11}(r, t) = e^{i\tilde{\omega}_1 t} \langle \tilde{1} | a_r | \phi_{out} \rangle = \langle \tilde{1} | a_r(t) | \phi_{in} \rangle$. Substituting Eq. (A5) into this equation, we obtain

$$\xi_{11}(\omega) = \frac{g_{11}(r, t)}{f(r-t)} = 1 - \frac{\kappa \sin^2 \theta_t}{\kappa/2 - i(\omega - \tilde{\omega}_{31})} - \frac{\kappa \cos^2 \theta_t}{\kappa/2 - i(\omega - \tilde{\omega}_{41})}. \quad (\text{A14})$$

Thus, $\xi_{11}(\omega)$ [Eq. (12)] is derived. ξ_{12} , ξ_{21} and ξ_{22} are derivable similarly.

Appendix B: averaged gate fidelity

Here, we present the formalism for evaluation of the averaged gate fidelity of the atom-photon gate. Considering the finite pulse length of the input pulse, the input state vectors are written as

$$|\tilde{1}, \omega_l^*\rangle_{in} = \int d\omega f_{\omega_l^*}(\omega) |\tilde{1}, \omega\rangle, \quad (\text{B1})$$

$$|\tilde{1}, \omega_h^*\rangle_{in} = \int d\omega f_{\omega_h^*}(\omega) |\tilde{1}, \omega\rangle, \quad (\text{B2})$$

$$|\tilde{2}, \omega_l^*\rangle_{in} = \int d\omega f_{\omega_l^*}(\omega) |\tilde{2}, \omega\rangle, \quad (\text{B3})$$

$$|\tilde{2}, \omega_h^*\rangle_{in} = \int d\omega f_{\omega_h^*}(\omega) |\tilde{2}, \omega\rangle, \quad (\text{B4})$$

where $f_{\omega_l^*}(\omega)$ is the wavefunction of the input photon in the frequency space. It is given, as the Fourier transform of Eq. (23) with $\omega = \omega_l^*$, by

$$f_{\omega_l^*}(\omega) = \sqrt{\frac{4\pi}{l^3}} \frac{1}{(\pi/l)^2 - (\omega - \omega_l^*)^2} \cos[(\omega - \omega_l^*)l/2], \quad (\text{B5})$$

where l denotes the pulse length. $f_{\omega_h^*}(\omega)$ is defined similarly.

After reflection of the input photon, the state vectors evolve as Eqs. (10)–(11). We also consider here the decay of the atomic excited state $|e\rangle$ during the gate time t_g . Using Eqs. (2) and (3), and denoting the atomic lifetime by T_1 , the dressed states $|\tilde{1}\rangle$ and $|\tilde{2}\rangle$ evolve as

$$|\tilde{1}\rangle \rightarrow |\tilde{1}'\rangle = \cos \theta_l |g, 0\rangle - e^{-t_g/2T_1} \sin \theta_l |e, 0\rangle + \dots, \quad (\text{B6})$$

$$|\tilde{2}\rangle \rightarrow |\tilde{2}'\rangle = \sin \theta_l |g, 0\rangle + e^{-t_g/2T_1} \cos \theta_l |e, 0\rangle + \dots, \quad (\text{B7})$$

where the dots denote the decayed states, which are entangled with the environment and are out of the considered Hilbert space. Omitting the phase factor due to natural evolution, the input state vectors evolve as

$$|\tilde{1}, \omega_l^*\rangle_{in} \rightarrow |\tilde{1}, \omega_l^*\rangle_{out} = \int d\omega f_{\omega_l^*}(\omega) \xi_{11}(\omega) |\tilde{1}', \omega\rangle + \dots, \quad (\text{B8})$$

$$|\tilde{1}, \omega_h^*\rangle_{in} \rightarrow |\tilde{1}, \omega_h^*\rangle_{out} = \int d\omega f_{\omega_h^*}(\omega) \xi_{11}(\omega) |\tilde{1}', \omega\rangle + \int d\omega f_{\omega_h^*}(\omega) \xi_{12}(\omega) |\tilde{2}', \omega - \Delta\omega\rangle, \quad (\text{B9})$$

$$|\tilde{2}, \omega_l^*\rangle_{in} \rightarrow |\tilde{2}, \omega_l^*\rangle_{out} = \int d\omega f_{\omega_l^*}(\omega) \xi_{21}(\omega) |\tilde{1}', \omega + \Delta\omega\rangle + \int d\omega f_{\omega_l^*}(\omega) \xi_{22}(\omega) |\tilde{2}', \omega\rangle, \quad (\text{B10})$$

$$|\tilde{2}, \omega_h^*\rangle_{in} \rightarrow |\tilde{2}, \omega_h^*\rangle_{out} = \int d\omega f_{\omega_h^*}(\omega) \xi_{22}(\omega) |\tilde{2}', \omega\rangle + \dots, \quad (\text{B11})$$

where the dots denote irrelevant terms that are out of the considered Hilbert space.

On the other hand, the ideal time evolution of the SWAP gate is

$$|\tilde{1}, \omega_l^*\rangle_{\text{in}} \rightarrow |\tilde{1}, \omega_l^*\rangle_{\text{out}}^{\text{id}} = |\tilde{1}, \omega_l^*\rangle_{\text{in}} = \int d\omega f_{\omega_l^*}(\omega) |\tilde{1}, \omega\rangle, \quad (\text{B12})$$

$$|\tilde{1}, \omega_h^*\rangle_{\text{in}} \rightarrow |\tilde{1}, \omega_h^*\rangle_{\text{out}} = |\tilde{2}, \omega_l^*\rangle_{\text{in}} = \int d\omega f_{\omega_l^*}(\omega) |\tilde{2}, \omega\rangle, \quad (\text{B13})$$

$$|\tilde{2}, \omega_l^*\rangle_{\text{in}} \rightarrow |\tilde{2}, \omega_l^*\rangle_{\text{out}} = |\tilde{1}, \omega_h^*\rangle_{\text{in}} = \int d\omega f_{\omega_h^*}(\omega) |\tilde{1}, \omega\rangle, \quad (\text{B14})$$

$$|\tilde{2}, \omega_h^*\rangle_{\text{in}} \rightarrow |\tilde{2}, \omega_h^*\rangle_{\text{out}} = |\tilde{2}, \omega_h^*\rangle_{\text{in}} = \int d\omega f_{\omega_h^*}(\omega) |\tilde{2}, \omega\rangle. \quad (\text{B15})$$

The entanglement fidelity is given by $f_{\text{sw}} = |\langle \text{id}_{\text{out}}(\tilde{1}, \omega_l^* | \tilde{1}, \omega_l^*)_{\text{out}} + \dots + \text{id}_{\text{out}}(\tilde{2}, \omega_h^* | \tilde{2}, \omega_h^*)_{\text{out}}|^2/16$, and the averaged gate fidelity of SWAP gate is given by $\mathcal{F}_{\text{sw}} = (4f_{\text{sw}} + 1)/5$ [26]. The fidelities of the other gates are obtained by replacing the right-hand sides of Eqs. (B12)–(B15) properly.

- [1] A. G. Fowler, M. Mariantoni, J. M. Martinis, and A. N. Cleland, *Phys. Rev. A* **86**, 032324 (2012).
- [2] R. Barends, J. Kelly, A. Megrant, A. Veitia, D. Sank, E. Jeffrey, T. C. White, J. Mutus, A. G. Fowler, B. Campbell, Y. Chen, Z. Chen, B. Chiaro, A. Dunsworth, C. Neill, P. O'Malley, P. Roushan, A. Vainsencher, J. Wenner, A. N. Korotkov, A. N. Cleland, and J. M. Martinis, *Nature* **508**, 500 (2014).
- [3] A. Yu. Kitaev, arXiv:quant-ph/9511026.
- [4] T. Monz, D. Nigg, E. A. Martinez, M. F. Brandl, P. Schindler, R. Rines, S. X. Wang, I. L. Chuang, and R. Blatt, *Science* **351**, 1068 (2016).
- [5] J. I. Cirac, A. K. Ekert, S. F. Huelga, and C. Macchiavello, *Phys. Rev. A* **59**, 4249 (1999).
- [6] A. Serafini, S. Mancini, and S. Bose, *Phys. Rev. Lett.* **96**, 010503 (2006).
- [7] H. J. Kimble, *Nature*, **453**, 1023 (2008).
- [8] N. H. Nickerson, Y. Li, and S. C. Benjamin, *Nat. Commun.* **4**, 1756 (2013).
- [9] C. Monroe, R. Raussendorf, A. Ruthven, K. R. Brown, P. Maunz, L.-M. Duan, and J. Kim, *Phys. Rev. A* **89**, 022317 (2014).
- [10] S. Debnath, N. M. Linke, C. Figgatt, K. A. Landsman, K. Wright, C. Monroe, arXiv:1603.04512.
- [11] L. M. Duan and H. J. Kimble, *Phys. Rev. Lett.* **92**, 127902 (2004).
- [12] A. Reiserer and G. Rempe, *Rev. Mod. Phys.* **87**, 1379 (2015).
- [13] B. Hacker, S. Welte, G. Rempe, and S. Ritter arXiv:1605.05261
- [14] D. Pinotsi and A. Imamoglu, *Phys. Rev. Lett.* **100**, 093603 (2008).
- [15] I. Shomroni, S. Rosenblum, Y. Lovsky, O. Bechler, G. Guendelman, and B. Dayan, *Science* **345**, 903 (2014).
- [16] K. Koshino, S. Ishizaka, and Y. Nakamura, *Phys. Rev. A* **82**, 010301(R) (2010).
- [17] A. Blais, R.-S. Huang, A. Wallraff, S. M. Girvin, and R. J. Schoelkopf, *Phys. Rev. A* **69**, 062320 (2004).
- [18] A. Wallraff, D. I. Schuster, A. Blais, L. Frunzio, R.-S. Huang, J. Majer, S. Kumar, S. M. Girvin, and R. J. Schoelkopf, *Nature* **431**, 162 (2004).
- [19] A. Narla, S. Shankar, M. Hatridge, Z. Leghtas, K. M. Sliwa, E. Zolys-Geller, S. O. Mundhada, W. Pfaff, L. Frunzio, R. J. Schoelkopf, and M. H. Devoret, *Phys. Rev. X* **6**, 031036 (2016).
- [20] D. L. Moehring, P. Maunz, S. Olmschenk, K. C. Younge, D. N. Matsukevich, L.-M. Duan, and C. Monroe, *Nature* **449**, 68 (2007).
- [21] K. Koshino, K. Inomata, T. Yamamoto and Y. Nakamura, *Phys. Rev. Lett.* **111**, 153601 (2013).
- [22] K. Inomata, K. Koshino, Z. R. Lin, W. D. Oliver, J. S. Tsai, Y. Nakamura and T. Yamamoto, *Phys. Rev. Lett.* **113**, 063604 (2014).
- [23] K. Inomata, Z. R. Lin, K. Koshino, W. D. Oliver, J. S. Tsai, T. Yamamoto, and Y. Nakamura, *Nat. Commun.* **7**, 12303 (2016).
- [24] D. Loss and D. P. DiVincenzo, *Phys. Rev. A* **57**, 120 (1998).
- [25] M. Pechal, L. Huthmacher, C. Eichler, S. Zeytinoglu, A. A. Abdumalikov, Jr., S. Berger, A. Wallraff, and S. Filipp, *Phys. Rev. X* **4**, 041010 (2014).
- [26] M. A. Nielsen, *Phys. Lett. A* **303**, 249 (2002).